J|A|C|S ARTICLES

Published on Web 08/20/2009

New Insights into ETS-10 and Titanate Quantum Wire: A Comprehensive Characterization

Nak Cheon Jeong,[†] Young Ju Lee,[†] Jung-Hyun Park,[‡] Hyunjin Lim,[§] Chae-Ho Shin,[‡] Hyeonsik Cheong,[§] and Kyung Byung Yoon*,[†]

Center for Nano Materials, Departments of Chemistry and Physics, Program of Integrated Biotechnology, Sogang University, Seoul 121−742, Korea, and Department of Chemical Engineering, Chungbuk National University, Cheongju, Chungbuk 361−763, Korea

Received May 11, 2009; E-mail: yoonkb@sogang.ac.kr

Abstract: The titanate quantum wires in ETS-10 crystals remain intact during ion exchange of the pristine cations ($Na^+_{0.47} + K^+_{0.53}$) with M^{n+} ions ($M^{n+} = Na^+$, K^+, Mg^{2+}, Ca^{2+}, Sr^{2+}, Ba^{2+}, Pb^{2+}, Cd^{2+}, Zn^{2+}) and during reverse exchange of the newly exchanged cations with Na^+. The binding energies of O(1s) and Ti(2p) decrease as the electronegativity of the cation decreases, and they are inversely proportional to the negative partial charge of the framework oxygen [$-\delta(O_f)$]. At least five different oxygen species were identified, and their binding energies (526.1−531.9 eV) indicate that the titanate-forming oxides are much more basic than those of aluminosilicate zeolites (530.2−533.3 eV), which explains the vulnerability of the quantum wire to acids and oxidants. The chemical shifts of the five NMR-spectroscopically nonequivalent Si sites, $\delta(I_A)$, $\delta(I_B)$, $\delta(II_A)$, $\delta(II_B)$, and $\delta(III)$, shift downfield as $-\delta(O_f)$ increases, with slopes of 2.5, 18.6, 133.5, 216.3, and 93.8 ppm/[$-\delta(O_f)$], respectively. The nonuniform responses of the chemical shifts to $-\delta(O_f)$ arise from the phenomenon that the cations in the 12-membered-ring channels shift to the interiors of the cages surrounded by four seven-membered-ring windows. On the basis of the above, we assign $\delta(I_A)$, $\delta(I_B)$, $\delta(II_A)$, and $\delta(II_B)$ to the chemical shifts arising from Si(12,12), Si(12,7), Si(7,12), and Si(7,7) atoms, respectively. The frequency of the longitudinal stretching vibration of the titanate quantum wire increases linearly and the bandwidth decreases nonlinearly with increasing $-\delta(O_f)$, indicating that the titanate quantum wire resembles a metallic carbon nanotube. As the degree of hydration increases, the vibrational frequency shifts linearly to higher frequencies while the bandwidth decreases. We identified another normal mode of vibration of the quantum wire, which vibrates in the region of 274−280 cm^{-1}. In the dehydrated state, the band-gap energy and the first absorption maximum shift to lower energies as $-\delta(O_f)$ increases, indicating the oxide-to-titanium(IV) charge-transfer nature of the transitions.

Introduction

ETS-10 is a highly intriguing nanoporous titanosilicate[1] that has shown the potential to work as an effective catalyst for various reactions, such as dehydration of *tert*-butyl alcohol to isobutene,[2] aldol condensation of acetone,[3] oxidative dehydrogenation of cyclohexanol,[4] production of propylene carbonate from carbon dioxide and propylene oxide,[5] and aromatization of *n*-hexane.[6] It is also an effective material for the selective removal of harmful heavy-metal ions[7−9] and photocatalytic removal of organic pollutants[10] and has also been tested as a material for solar cells.[11] However, the most interesting feature that makes ETS-10 so unique is that it contains periodically positioned quantum wires [−O−Ti(O−)$_4$−O−] with a diameter (d) of ∼0.67 nm running along the two perpendicular directions in the crystal (Chart 1A).[1,12−17]

[†] Department of Chemistry, Sogang University.
[‡] Chungbuk National University.
[§] Department of Physics, Sogang University.

(1) (a) Kuznicki, S. M. U.S. Patent 4,853,202, 1989. (b) Anderson, M. W.; Terasaki, O.; Ohsuna, T.; Philippou, A.; MacKay, S. P.; Ferreira, A.; Rocha, J.; Lidin, S. *Nature* **1994**, *367*, 347–351. (c) Anderson, M. W.; Terasaki, O.; Ohsuna, T.; Malley, P. J. O.; Philippou, A.; MacKay, S. P.; Ferreira, A.; Rocha, J.; Lidin, S. *Philos. Mag. B* **1995**, *71*, 813–841.
(2) Philippou, A.; Naderi, M.; Rocha, J.; Anderson, M. W. *Catal. Lett.* **1998**, *53*, 221–224.
(3) Philippou, A.; Anderson, M. W. *J. Catal.* **2000**, *189*, 395–400.
(4) Valente, A.; Lin, Z.; Brandão, P.; Portugal, I.; Anderson, M. W.; Rocha, J. *J. Catal.* **2001**, *200*, 99–105.
(5) Doskocil, E. J. *J. Phys. Chem. B* **2005**, *109*, 2315–2320.
(6) Waghmode, S. B.; Vetrivel, R.; Gohinath, C. S.; Sivasanker, S. *J. Phys. Chem. B* **2004**, *108*, 11541–11548.
(7) (a) Lv, L.; Tsoi, G.; Zhao, X. S. *Ind. Eng. Chem. Res.* **2004**, *43*, 7900–7906. (b) Zhao, X. S.; Lee, J. L.; Chia, P. A. *Langmuir* **2003**, *19*, 1977–1979. (c) Lv, L.; Wang, K.; Zhao, X. S. *J. Colloid Interface Sci.* **2007**, *305*, 218–225.
(8) (a) Choi, J. H.; Kim, S. D.; Noh, S. H.; Oh, S. J.; Kim, W. J. *Microporous Mesoporous Mater.* **2006**, *87*, 163–169. (b) Choi, J. H.; Kim, S. D.; Kwon, Y. J.; Kim, W. J. *Microporous Mesoporous Mater.* **2006**, *96*, 157–167.
(9) Lopes, C. B.; Otero, M.; Coimbra, J.; Pereira, E.; Rocha, J.; Lin, Z.; Duarte, A. *Microporous Mesoporous Mater.* **2007**, *103*, 325–332.
(10) Luca, V.; Osborne, M.; Sizgek, D.; Griffith, C.; Araujo, P. Z. *Chem. Mater.* **2006**, *18*, 6132–6138.
(11) Atíenzar, P.; Valencia, S.; Corma, A.; García, H. *ChemPhysChem* **2007**, *8*, 1115–1119.
(12) Jeong, N. C.; Lee, M. H.; Yoon, K. B. *Angew. Chem., Int. Ed.* **2007**, *46*, 5868–5872.

10.1021/ja903638v CCC: $40.75

Chart 1. (A) Illustration of 3D Networks of Titanate (TiO_3^{2-}) Quantum Wires (red) and SiO_2 Channels (gray) in a Truncated-Bipyramidal ETS-10 crystal with Polymorph B and (B, C) Single Titanate Quantum Wires Charge-Balanced with (B) Hydrated and (C) Naked Cations

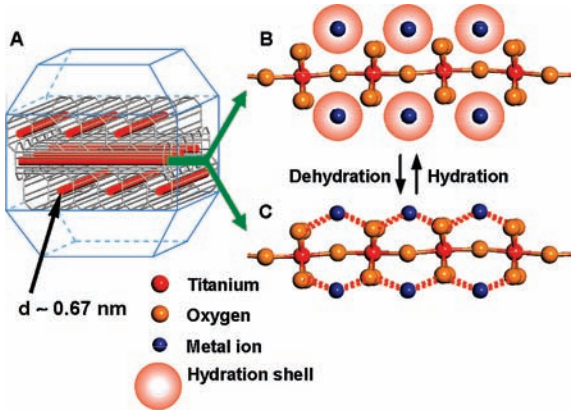

Among the known quantum wires,[18,19] the TiO_3^{2-} quantum wire is an anionic counterpart of anatase nanowire[18] and can be regarded as a one-dimensional (1D) extreme of three-dimensional (3D) bulk titanates, which are widely used in industry as capacitors, etc.[20] Therefore, acquiring the properties of the TiO_3^{2-} quantum wire also means acquiring the 1D-extreme properties of titanates. Each TiO_3^{2-} quantum wire is surrounded by insulating nanoporous silica with a pore size of 8 Å × 5 Å, and the wires are supramolecularly organized within the crystalline solid from its birth. It exhibits the quantum confinement effect along the chain direction even at length scales longer than 50 nm.[12] The estimated reduced mass of an exciton along its chain direction (μ_z, $0.0006m_e$)[12] is much smaller than those of InSb ($0.014m_e$)[21] and single-walled carbon nanotubes (SW-CNTs, $0.019m_e$).[22] Such an unusually small μ_z further suggests the possibility that the carrier mobility along the TiO_3^{2-} molecular wire, despite the wire's oxide nature, can be much greater than that in single-walled carbon nanotubes, indicating the possibility that the quantum wire is metallic.

The unit cell composition of ETS-10 is $M^{n+}_{(2/n)}Ti_1Si_5O_{13}$. Thus, like aluminosilicate zeolites, ETS-10 also carries charge-balancing cations to compensate for the negative charges of the titanate quantum wires. In the related aluminosilicate zeolites, the (negative) charge density of the framework[23] has often been represented by the binding energy of an O 1s electron,[24] despite the fact that it is a core electron. However, the Sanderson partial (negative) charge of the framework oxygen, $-\delta(O_f)$, has often been used instead of the O 1s binding energy because the binding energy of an O 1s electron cannot be routinely obtained and it has been established that the two values [the O 1s binding energy and $-\delta(O_f)$] are linearly correlated.[24,25]

Scheme 1

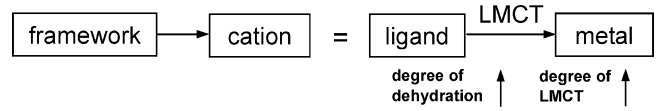

The negative charge density of the framework can be conveniently tuned by varying both the type of charge-balancing cation and the degree of dehydration of the zeolite because the framework oxygen atoms interact with the cations through a ligand-to-metal charge-transfer (LMCT) interaction (Scheme 1) and the degree of the LMCT interaction increases as the degree of dehydration increases.[25,26]

Thus, in a dry zeolite, the framework charge density decreases as the acceptor strength or the electronegativity of the charge-balancing cation increases and also as the degree of dehydration increases, since dehydration of the zeolite leads to the removal of water shells from the cations, thereby increasing the degree of direct LMCT from the framework to the cation in the ground state.

Normally, a mixture of Na^+ and K^+ exists within the pristine ETS-10 crystals for charge neutralization. It has been believed that the charge-balancing cations are evenly distributed along the quantum wire in the vicinity of each titanium center (Chart 1B).[27] They can be exchanged with other cations through ion exchange in aqueous solution.[7,9,15,28−30] In the hydrated state, the cations are also expected to be at least partially surrounded by water molecules, as illustrated in Chart 1B. In the dehydrated state, however, they should be directly coordinated by the framework oxygen atoms, as illustrated in Chart 1C. Accord-

(13) (a) Borello, E.; Lamberti, C.; Bordiga, S.; Zecchina, A.; Areán, C. O. *Appl. Phys. Lett.* **1997**, *71*, 2319–2321. (b) Llabrés i Xamena, F. X.; Damin, A.; Bordiga, S.; Zecchina, A. *Chem. Commun.* **2003**, 1514–1515. (c) Damin, A.; Llabrés i Xamena, F. X.; Lamberti, C.; Civalleri, B.; Zicovich-Wilson, C. M.; Zecchina, A. *J. Phys. Chem. B* **2004**, *108*, 1328–1336. (d) Bordiga, S.; Palomino, G. T.; Zecchina, A.; Ranghino, G.; Giamello, E.; Lamberti, C. *J. Chem. Phys.* **2000**, *112*, 3859–3867.
(14) Zimmerman, A. M.; Doren, D. J.; Lobo, R. F. *J. Phys. Chem. B* **2006**, *110*, 8959–8964.
(15) Lamberti, C. *Microporous Mesoporous Mater.* **1999**, *30*, 155–163.
(16) Wang, X.; Jacobson, A. J. *Chem. Commun.* **1999**, 973–974.
(17) Yilmaz, B.; Warzywoda, J.; Sacco, A., Jr. *Nanotechnology* **2006**, *17*, 4092–4099.
(18) (a) Liu, C.; Yang, S. *ACS Nano* **2009**, *3*, 1025–1031. (b) Venkataraman, L.; Lieber, C. M. *Phys. Rev. Lett.* **1999**, *83*, 5334–5337. (c) Huang, Y.; Duan, X.; Cui, Y.; Lauhon, L. J.; Kim, K.-H.; Lieber, C. M. *Science* **2001**, *294*, 1313–1317. (d) Duan, X.; Huang, Y.; Cui, Y.; Wang, J.; Lieber, C. M. *Nature* **2001**, *409*, 66–69.
(19) (a) Xia, Y.; Yang, P.; Sun, Y.; Wu, Y.; Mayers, B.; Gates, B.; Yin, Y.; Kim, F.; Yan, H. *Adv. Mater.* **2003**, *15*, 353–389. (b) Golden, J. H.; DiSalvo, F. J.; Fréchet, J. M. J.; Silcox, J.; Thomas, M.; Elman, J. *Science* **1996**, *273*, 782–784. (c) Yu, H.; Li, J.; Loomis, R. A.; Wang, L.-W.; Buhro, W. E. *Nat. Mater.* **2003**, *2*, 517–520.
(20) Bavykin, D. V.; Friedrich, J. M.; Walsh, F. C. *Adv. Mater.* **2006**, *18*, 2807–2824.
(21) Burs, L. E. *J. Chem. Phys.* **1984**, *80*, 4403–4409.
(22) Pedersen, T. G. *Phys. Rev. B* **2003**, *67*, 073401.
(23) It is more often called the framework electron donor strength or framework basicity. These terms eventually represent the richness of the electron density in the framework. Among these, the terms electron donor strength and framework basicity should rather be used when one deals with the interaction between the framework and its counterparts such as electron acceptors and acids. Therefore, in this work, we use negative framework charge density to represent the richness of electron density.
(24) Huang, H.; Adnot, A.; Kaliaguine, S. *J. Am. Chem. Soc.* **1992**, *114*, 10005–10010.
(25) (a) Mortier, W. J.; Schoonheydt, R. A. *Prog. Solid State Chem.* **1985**, *16*, 1–125. (b) Heidler, R.; Janssens, G. O. A.; Mortier, W. J.; Schoonheydt, R. A. *J. Phys. Chem.* **1996**, *100*, 19728–19734. (c) Genechten, K. A. V.; Mortier, W. J. *Zeolites* **1988**, *8*, 273–283.
(26) (a) Yoon, K. B. In *Handbook of Zeolite Science and Technology*; Auerbach, S. M., Carrado, K. A., Dutta, P. K., Eds.; Marcel Dekker: New York, 2003; Chapter 13. (b) Park, Y. S.; Um, S. Y.; Yoon, K. B. *J. Am. Chem. Soc.* **1999**, *121*, 3193–3200. (c) Choi, S. Y.; Park, Y. S.; Hong, S. B.; Yoon, K. B. *J. Am. Chem. Soc.* **1996**, *118*, 9377–9386.
(27) (a) Anderson, M. W.; Agger, J. R.; Luigi, D.-P.; Baggaley, A. K.; Rocha, J. *Phys. Chem. Chem. Phys.* **1999**, *1*, 2287–2282. (b) Grillo, M. E.; Carrazza, J. *J. Phys. Chem.* **1996**, *100*, 12261–12264.
(28) Krisnandi, Y. K.; Lachowski, E. E.; Howe, R. F. *Chem. Mater.* **2006**, *18*, 928–933.
(29) Waghmode, S. B.; Vetrivel, R.; Hegde, S. G.; Gopinath, C. S.; Sivasanker, S. *J. Phys. Chem. B* **2003**, *107*, 8517–8523.
(30) Pavel, C. C.; Zibrowius, B.; Löffler, E.; Schmidt, W. *Phys. Chem. Chem. Phys.* **2007**, *9*, 3440–3446.

ingly, the degree of intimate LMCT interaction in Scheme 1 increases as the degree of dehydration of the zeolite increases, and it reaches a maximum in the fully dehydrated state.

With the above background in mind, we have addressed the following questions: Would the electronegativity of the charge-balancing cation and the degree of hydration of the molecular sieve also affect the charge density of the TiO_3^{2-} quantum wires and the silicon atoms that surround them? If yes, how would the charge density on the titanate quantum wires affect their band-gap energy (E_g), vibrational frequency, and vibrational bandwidth? Since ion exchange of Na^+ and K^+ of the pristine ETS-10 with NH_4^+ and H^+ readily decomposes the titanate quantum wire[28,31] while ion exchange of the cations with Cs^+ can be done reversibly without decomposing it,[30] are there other cations that could be reversibly exchanged into ETS-10 without decomposing the quantum wires?

We now report the ion exchange behavior of ETS-10, the effect of the electronegativity and degree of dehydration of the cation on the charge densities of the Ti, O, and Si atoms, and the effect of negative charge density in the titanate quantum wire on its E_g, vibrational frequency, and vibrational bandwidth. We also report the XPS spectrum of Ti, the detailed assignment of ^{29}Si NMR peaks to the silicon sites, and the valuable information that the cations in the 12-memberd-ring (12MR) channels move to the cages surrounded by four seven-membered-ring (7MR) windows in the dehydrated state and that the framework oxides in ETS-10 are much more basic than those in zeolites.

Experimental Section

Synthesis of ETS-10. ETS-10 crystals with the sizes of ~500 nm were prepared according to the previously reported procedure.[32] The composition of pristine ETS-10 is $Na_{0.94}K_{1.06}TiSi_5O_{13}$. Thus, the cations in pristine ETS-10 are a mixture of Na^+ and K^+ in the ratio of 0.94:1.06. Hereafter, the pristine cations are represented by the expression $Na^+_{0.47} + K^+_{0.53}$.

Preparation of M^{n+}-Exchanged ETS-10 Crystals (M^{n+}-ETS-10, M^{n+} = Na^+, K^+, Mg^{2+}, Ca^{2+}, Sr^{2+}, Ba^{2+}, Pb^{2+}, Cd^{2+}, Zn^{2+}). ETS-10 samples exchanged with ten different metal ions (M^{n+}-ETS-10) were prepared by exchanging Na^+ and K^+ cations in pristine ETS-10 with the desired metal ion using the corresponding salt [NaCl, KCl, $MgCl_2$ $CaCl_2$, $SrCl_2$, $BaCl_2$, $Pb(CH_3CO_2)_2$, $Cd(CH_3CO_2)_2$, or $Zn(CH_3CO_2)_2$]. The ion exchange was carried out by introducing 1 g of pristine ETS-10 powder into 45 mL of a 2 M aqueous solution of the salt at room temperature and then stirring for 1 h at room temperature. The ion exchange was repeated two more times to achieve the highest possible degree of ion exchange. Although the ion exchange did not go to completion, we denote the ion-exchanged ETS-10 as M^{n+}-ETS-10, where M^{n+} is the major cation (Na^+, $Na^+ + K^+$, K^+, Mg^{2+}, Ca^{2+}, Sr^{2+}, Ba^{2+}, Pb^{2+}, Cd^{2+}, or Zn^{2+}). The compositions of cations in each M^{n+}-ETS-10 are listed in Table SI 1 in the Supporting Information. For the ion exchange of Na^+ with K^+ ion in pristine ETS-10, the K^+ content in ETS-10 was first decreased to ~20%, after which ion exchange of the 80% Na^+ ion with K^+ ion was carried out. Likewise, the Na^+ content was first decreased to 20% before the ion exchange of Na^+ with K^+ was carried out.

Preparation of Na^+-Reverse-Exchanged ETS-10. To check the stability of the titanate quantum wires during and after ion exchange, we reverse-exchanged each M^{n+} in M^{n+}-ETS-10 with Na^+ ion. For this, 0.5 g of M^{n+}-ETS-10 was introduced into the saturated NaCl solution (45 mL), and the solution was shaken for 1 day at room temperature. The reverse ion exchange was repeated two more times. Despite this, the degree of reverse exchange was not complete, as summarized in Table SI 2 in the Supporting Information.

Dehydration of M^{n+}-ETS-10 Samples. Since the M-ETS-10 samples were not stable above 250 °C (Figure SI 1 in the Supporting Information), they were dried at 250 °C for 4 h under vacuum ($<10^{-6}$ Torr). For the measurements of magic-angle-spinning (MAS) solid-state ^{29}Si NMR spectra, the dried M^{n+}-ETS-10 samples were treated with octadecytrichlorosilane in a glovebox according to the procedure described in our previous report.[33]

Preparation of Partially Hydrated M^{n+}-ETS-10. Dry M^{n+}-ETS-10 powder (~200 mg) was spread onto a light, shallow, plastic container (40 mm × 40 mm) placed on top of a microbalance, and the weight was quickly measured after a desired period of time. After the weight measurement, the powder was then quickly transferred into a flat, round, fused silica cell (i.d. = 19 mm), and Raman and UV−vis spectra were measured immediately. After the spectral measurements, the powder was spread back onto the weighing container and allowed to pick up more moisture from the atmosphere. After a desired period of exposure to the atmosphere, the weight increase was measured using a microbalance, and the powder was subsequently transferred into a fused silica cell for the measurements of Raman and UV−vis spectra.

3D Bulk Titanates. Li_2TiO_3, $BaTiO_3$, $SrTiO_3$, and $PbTiO_3$ were purchased from Aldrich. $CaTiO_3$ was prepared by thoroughly grinding a 1:1 mixture of $CaCO_3$ (1 g, Aldrich) and TiO_2 (0.8 g, Aldrich) at room temperature and subsequently heating at 1000 °C for 16 h.

Instrumentation. Scanning electron microscopy (SEM) images were obtained using a field-effect scanning electron microscope (Hitachi S-4300) operating at an acceleration voltage of 20 kV. Elemental analyses of various M^{n+}-ETS-10 samples for M^{n+}, Si, and Ti were carried out by analyzing the energy-dispersive X-ray (EDX) spectra of the samples using a Horiba EMAX 6853-H EDX spectrometer. Comparison of some of our elemental analysis results with those obtained from chemical analysis showed good matching, supporting the accuracy of the EDX analyses in this report. Powder X-ray diffraction (XRD) patterns were obtained using a Rigaku D/MAX-2500/pc diffractometer. Raman spectra of the samples were recorded on a homemade setup equipped with an Ar^+ ion laser (Spectra-Physics Stabilite 2017) as an excitation beam source, a spectrometer (Horiba Jobin Yvon TRIAX 550), and a CCD detector (Horiba Jobin Yvon Symphony) cooled to −133 °C. The wavelength of the excitation beam was 514.5 nm. Diffuse-reflectance UV−vis spectra of the samples were recorded on a Varian Cary 5000 UV−vis−NIR spectrophotometer equipped with an integrating sphere. Barium sulfate was used as the reference. The diffuse-reflectance spectra were converted into the Kubelka−Munk (K−M) formalism. X-ray photoelectron spectroscopy (XPS) of M^{n+}-ETS-10 samples (for M^{n+} = Na^+, K^+, Ca^{2+}, Sr^{2+}, Ba^{2+}) were recorded on a VG Scientifics ESCALAB 250 XPS spectrometer at the Korea Basic Science Institute located at Pusan National University. The Brunauer-Emmett-Teller (BET) surface area, micropore volume, and total pore volume were obtained from argon adsorption at 87.3 K using a volumetric method with a Micromeritics ASAP 2020 analyzer. Micropore volume was determined using the t-plot method. Prior to adsorption of argon, the samples were evacuated under a vacuum of 3×10^{-5} Torr at 250 °C. The ^{29}Si MAS NMR spectra were measured on a Bruker Avance 500 spectrometer operating at a spinning rate of 10 kHz and a ^{29}Si frequency of 99.351 kHz using a $\pi/2$ rad pulse length of 8 μs. A long recycle of 30 s was used to avoid relaxation effects in the signal intensities, and

(31) (a) Lv, L.; Lee, F. Y.; Zhou, J.; Su, F.; Zhao, X. S. *Microporous Mesoporous Mater.* **2006**, *96*, 270–275. (b) Lv, L.; Zhou, J. K.; Su, F.; Zhao, X. S. *J. Phys. Chem. C* **2007**, *111*, 773–778.
(32) Jeong, N. C.; Lee, Y. J.; Yoon, K. B. *Microporous Mesoporous Mater.* **2008**, *115*, 308–313.
(33) (a) Jeong, N. C.; Kim, H. S.; Yoon, K. B. *Langmuir* **2005**, *21*, 6038–6047. (b) Jeong, N. C.; Kim, H. S.; Yoon, K. B. *J. Phys. Chem. C* **2007**, *111*, 10298–10312.

2500 pulse transients were typically accumulated. The ^{29}Si chemical shifts are referenced to tetramethylsilane (TMS).

Results and Discussion

Quality of the ETS-10 Crystals Used in This Study. ETS-10 has often been produced with seriously damaged (short) TiO_3^{2-}quantum wires.[17,34] Therefore, even if the XRD pattern of a newly prepared sample matches the standard diffraction pattern of ETS-10, this does not guarantee that high-quality TiO_3^{2-}molecular wires (i.e., with long lengths and no defects) were produced. The presence and quality (length) of the TiO_3^{2-}quantum wires in ETS-10 have often been analyzed by the longitudinal (along-the-wire) stretching vibration band of the TiO_3^{2-}molecular wire and its bandwidth in the Raman spectrum.[13b,17,28,30,31,34,35] In the hydrated pristine ETS-10 (with $Na^+_{0.47} + K^+_{0.53}$ as the countercations), when the lengths of the TiO_3^{2-} quantum wires are longer than ~50 nm and the quality of the titanate quantum wires is good, the longitudinal stretching vibration band remains constant at ~724 cm^{-1} with a bandwidth (fwhm) of ~26 cm^{-1}.[12] As the quality of the ETS-10 decreases (i.e., as the lengths of TiO_3^{2-} quantum wires become shorter than ~50 nm), the longitudinal stretching vibrational band is blue-shifted and the bandwidth (fwhm) increases.[13b,17,28,30,31,34,35] In this respect, the observation that the frequency and bandwidth of our pristine ETS-10 were 724 and 24 cm^{-1}, respectively, indicates that the titanate quantum wires in the ETS-10 crystals used in this study were produced with lengths of >50 nm with few defects.

Ion Exchange of Pristine ETS-10 with Several Metal Ions (M^{n+} = Na^+, K^+, Mg^+, Ca^{2+}, Sr^{2+}, Ba^{2+}, Pb^{2+}, Cd^{2+}, Zn^{2+}) and Reverse Exchange of M^{n+} with Na^+. The Sanderson electronegativities of the cations are as follows: $K^+ = 0.445$, $Na^+ = 0.560$, $Ba^{2+} = 0.651$, $Sr^{2+} = 0.721$, $Ca^{2+} = 0.950$, $Mg^{2+} = 1.318$, $Pb^{2+} = 1.920$, $Cd^{2+} = 1.970$, and $Zn^{2+} = 2.223$.[36] Thus, the Sanderson elctronegativity increases in the order $K^+ < Na^+ < Ba^{2+} < Sr^{2+} < Ca^{2+} < Mg^{2+} < Pb^{2+} < Cd^{2+} < Zn^{2+}$.

Nondestructive Forward Ion Exchange and High Affinity for Pb^{2+}, Cd^{2+}, and Zn^{2+}. The ion exchange seemed to reach equilibrium within 1 h at room temperature. The degree of ion exchange after the first cycle increased in the order Ba^{2+} (49) < Sr^{2+} (54) < [Ca^{2+} (63) ≈ Na^+ (64) ≈ K^+ (65) ≈ Mg^{2+} (67)] < [Zn^{2+} (76) ≈ Cd^{2+} (77) ≈ Pb^{2+} (79)] (Figure 1A and Table SI 1 in the Supporting Information). Consistent with the literature reports,[7,8a] Pb^{2+} was the most preferred cation after the first cycle. In general, ETS-10 showed higher preferences for Zn^{2+}, Cd^{2+}, and Pb^{2+} than for alkali and alkaline-earth metal ions. The degrees of ion exchange after the third cycle ranged between 80 and 94%, with specific values of 80% (Na^+, K^+, Mg^{2+}), 85−88% (Sr^{2+}, Ba^{2+}, Ca^{2+}), and 90−94% (Pb^{2+}, Cd^{2+}, Zn^{2+}). Thus, as noted, the ion exchange did not go to completion (100%) even after the ion exchange procedure was repeated three times, despite the fact that each cycle was carried out in a freshly prepared, highly concentrated (2 M) solution of the salt. The degrees of ion exchange for Pb^{2+}, Cd^{2+}, and Zn^{2+} were 90, 93, and 94%, respectively. Although the differences were small, the order of preference increased as $Pb^{2+} < Cd^{2+} < Zn^{2+}$, which coincides with the order of the increase in the Sanderson electronegativities. Analysis of the remaining alkali metal cations (Table SI 1 in the Supporting Information, fourth column) showed that between the two pristine cations, Na^+ and K^+, the former (Na^+) is more readily exchanged by other cations than the latter (K^+).

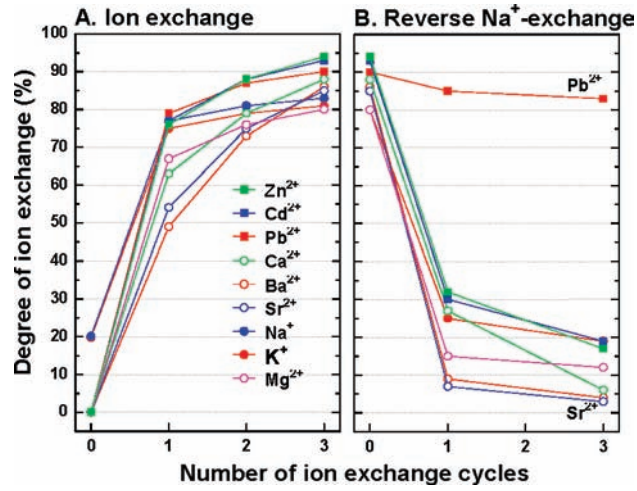

Figure 1. Plots of (A) the degrees of ion exchange of the pristine cations ($Na^+_{0.47} + K^+_{0.53}$) with M^{n+} [or ($Na^+_{0.8} + K^+_{0.2}$) for the ion exchange with K^+ or ($Na^+_{0.2} + K^+_{0.8}$) for the ion exchange with Na^+] and (B) the degrees of reverse ion exchange of M^{n+} with Na^+ with respect to the number of ion exchange cycles. The M^{n+} are listed in (A).

Reverse Ion Exchange and Special Affinity for Pb^{2+}. Reverse ion exchange of the newly introduced M^{n+} with Na^+ was also carried out three times for each M^{n+}-ETS-10. The degrees of reverse ion exchange (Figure 1B and Table SI 2 in the Supporting Information) were higher than 77% in all cases except $M^{n+} = Pb^{2+}$, for which the degree of reverse ion exchange was only 8%. This indicates that the ion exchange of the pristine metal ions (Na^+ and K^+) with Pb^{2+} is almost irreversible. The exchange of Pb^{2+} with the most preferred cation, Zn^{2+}, also did not occur readily. Thus, even after six ion exchange cycles with Zn^{2+}, the degree of ion exchange of Pb^{2+} with Zn^{2+} was only 20%. Ion exchange of the pristine cations with Pb^{2+} does not cause structural collapse (see the next section). Since Zn^{2+} is more preferred than Pb^{2+}, the difficulty of exchanging Pb^{2+} with not only Na^+ but also Zn^{2+} indicates that the back-exchange of Pb^{2+} with other cations is kinetically hindered.

Among the cations studied in this work, the alkaline-earth metal ions (Ba^{2+}, Sr^{2+}, Ca^{2+}, and Mg^{2+}) were most readily replaced by Na^+. This fact is consistent with the phenomenon that these cations were most reluctantly exchanged into ETS-10, indicating that ETS-10 has a relatively low affinity for the alkaline-earth metal ions, particularly the large cations Sr^{2+} and Ba^{2+}. The reverse-ion-exchanged ETS-10 samples are denoted as (M^{n+}→Na^+)ETS-10.

Powder XRD Patterns of M^{n+}-ETS-10 and (M^{n+}→Na^+) ETS-10. The powder XRD patterns of M^{n+}-ETS-10 were similar to that of the pristine ETS-10 in the hydrated state for all of the M^{n+} ions except Pb^{2+} and Cd^{2+} (Figure 2A), which showed minor variations. Thus, when $M^{n+} = Pb^{2+}$, the following took place: the intensity of the lowest-angle peak ($2\theta = 5.98°$) increased by a factor of ~2; a new peak at $2\theta = 15.23°$ appeared in significant intensity; the intensity of the peak at $2\theta = 17.86°$ increased significantly; the peak at 20.05° disappeared; the peaks at 23.69, 25.73, and 27.09° shifted to slightly lower angles (23.64, 25.66, and 27.01°, respectively) with accompanying intensity increases; and a new peak appeared at 26.69°. Similar changes were observed when $M^{n+} = Cd^{2+}$, except that even

(34) Southon, P. D.; Howe, R. F. *Chem. Mater.* **2002**, *14*, 4209–4218.
(35) Pavel, C. C.; Park, S.-H.; Dreier, A.; Tesche, B.; Schmidt, W. *Chem. Mater.* **2006**, *18*, 3813–3820.
(36) Sanderson, R. T. *J. Am. Chem. Soc.* **1983**, *105*, 2259–2261.

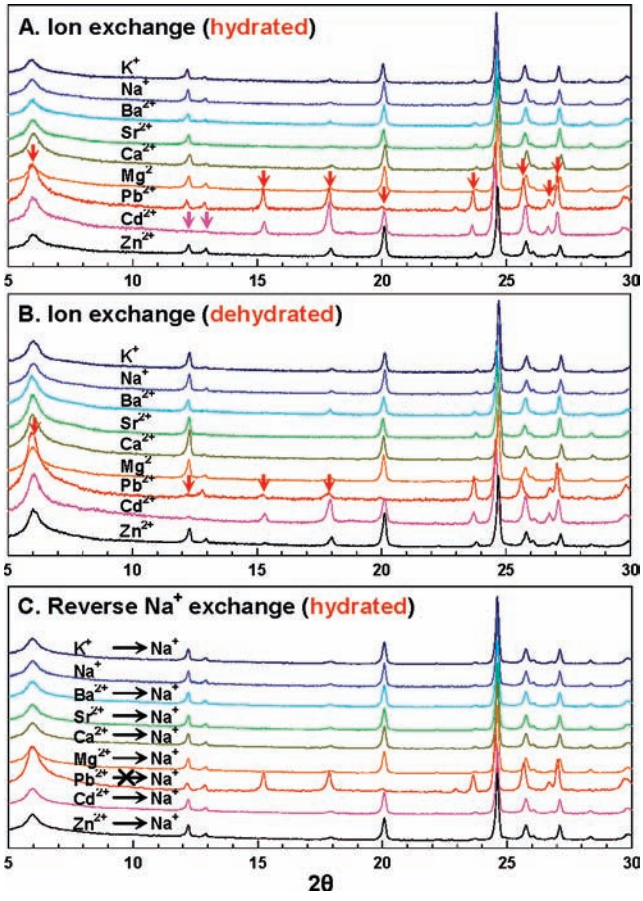

Figure 2. Powder XRD patterns of M^{n+}-ETS-10 in the (A) hydrated and (B) dehydrated states and of (C) (M^{n+}→Na^+)ETS-10 in the hydrated state.

the two small peaks at 12.20 and 12.92° disappeared, but the peak at 20.09° did not disappear and the peak at 25.76° did not shift to the lower-angle region. We ascribe the above changes to the presence of Pb^{2+} and Cd^{2+} ions on the regular positions in ETS-10 even in the hydrated states. Upon dehydration, when $M^{n+} = Pb^{2+}$, the intensity of the lowest-angle peak at $2\theta = 6.1°$ increased even further, and the peak at 12.20° disappeared; also, the intensities of the peaks at 15.23 and 17.86° decreased a bit (Figure 2B). However, when $M^{n+} = Cd^{2+}$, no further changes were observed.

Restoration of the Original Diffraction Patterns after Reverse Exchange with Na^+. Interestingly, except when $M^{n+} = Pb^{2+}$, the powder XRD patterns of the reverse-Na^+-exchanged ETS-10 samples [(M^{n+}→Na^+)ETS-10] returned to that of the pristine or Na^+-ETS-10 (Figure 2C). This result shows that ETS-10 retains its structural integrity during ion exchange with K^+, Na^+, Ba^{2+}, Sr^{2+}, Ca^{2+}, Mg^{2+}, and Zn^{2+} and reverse ion exchange with Na^+ in the dry or fully hydrated state. The above results also show that ETS-10 has an exceptionally high affinity for Pb^{2+}, as if this cation is very tightly encapsulated within the framework pockets, and as a result, the exchange of Na^+ and K^+ with Pb^{2+} is almost irreversible. Although Pb^{2+}-exchanged ETS-10 gives additional diffraction peaks, the existence of the original diffraction peaks of the pristine ETS-10 indicates that ETS-10 also does not undergo structural damage after exchange with Pb^{2+}, in contrast to its behavior with NH_4^+ and H^+.[28,31]

Argon Adsorption Isotherms of M^{n+}-ETS-10. No Indication of Mesopore Formation after Ion Exchange. We also obtained

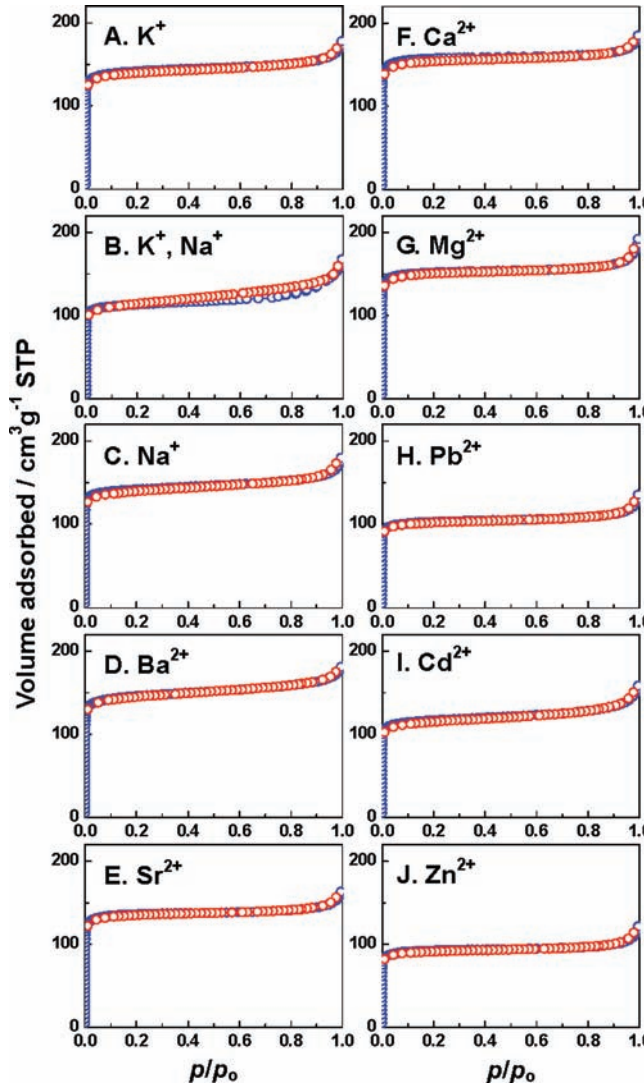

Figure 3. Ar adsorption isotherms of M^{n+}-ETS-10 for p/p_0 in the range 0.0−1.0.

argon BET isotherms of M^{n+}-ETS-10 samples in the region of relative pressure (p/p_o) between 10^{-6} and 1.0 (Figure 3) to check whether mesopores arising from structural damage are produced after ion exchange of the pristine cations in ETS-10 with various metal ions under the given exchange conditions (also see Figure SI 2 in the Supporting Information). In fact, this is the first report to systematically compare the argon BET isotherms of ETS-10 exchanged with various metal ions. The isotherms showed no sudden increases in adsorption volume and no hysteresis between adsorption and desorption for $p/p_o = 0.1-0.8$, indicating that the ion exchange does not cause the formation of mesopores. This result further confirms that the structure of ETS-10 is not damaged even partially either during or after ion exchange of the pristine cations with the above cations or even after dehydration.

The micropore volumes (in $cm^3\ g^{-1}$) ranged from 0.115 (Zn^{2+}) to 0.198 (Ca^{2+}) when measured using the t-plot method or from 0.141 (Zn^{2+}) to 0.240 (Ca^{2+}) when estimated by the value at $p/p_o = 0.12$ (Table SI 3 in the Supporting Information). The total pore volumes at $p/p_o = 0.99$ (in $cm^3\ g^{-1}$) ranged from 0.155 (Zn^{2+}) to 0.285 (Ca^{2+}). The differences between the total and micropore volumes were small and nearly constant (0.024−0.034). The BET surface areas (in $m^2\ g^{-1}$) were 554

(Ca^{2+}), 536 (Mg^{2+}), 507 (Ba^{2+}), 500 (Na^+), 496 (K^+), 480 (Sr^{2+}), 407 (Cd^{2+}), 396 ($Na^+_{0.47} + K^+_{0.53}$), 359 (Pb^{2+}), and 323 (Zn^{2+}). Interestingly, the surface areas of ETS-10 decreased significantly when the high-affinity cations (Zn^{2+}, Pb^{2+}, and Cd^{2+}) were the charge-balancing cations. The above results show that the size and number of cations sensitively affect the micropore volume and surface area, the cation exchange does not cause the formation of mesopores, and the micropores and the external surface of ETS-10 are the two constituents of the total surface area.

^{29}Si MAS NMR Spectra of M^{n+}-ETS-10 and ($M^{n+}\rightarrow Na^+$) ETS-10: Periodic Localization of Cations at the Cross Section of Titanate Quantum Wires in the Dehydrated State. Solid-state MAS ^{29}Si NMR spectra of M^{n+}-ETS-10 in both the hydrated (Figure 4A) and dehydrated (Figure 4B) states and ($M^{n+}\rightarrow Na^+$)ETS-10 in the hydrated state (Figure 4C) were obtained for $M^{n+} = K^+$, $Na^+_{0.47} + K^+_{0.53}$, Na^+, Ba^{2+}, and Sr^{2+}. The chemical shifts of the three observed peaks are listed in Table SI 4 in the Supporting Information. The ^{29}Si NMR spectra of dehydrated M^{n+}-ETS-10 could be resolved into the five chemical shifts $\delta(I_A)$, $\delta(I_B)$, $\delta(II_A)$, $\delta(II_B)$, and $\delta(III)$, as indicated in Figure 4B (bottom). The chemical shifts are tabulated in Table SI 5 in the Supporting Information. The linear relationships between the chemical shifts and the calculated $-\delta(O_f)$ values are shown in Figure 4D. The $-\delta(O_f)$ values for M^{n+}-ETS-10 were obtained from the chemical composition according to eq 1:

$$\delta(O_f) = \frac{^{i+j+k+19}\sqrt{S_M{}^i S_{Na}{}^j S_K{}^k S_{Ti}{}^1 S_{Si}{}^5 S_O{}^{13}} - S_O}{2.08\sqrt{S_O}} \quad (1)$$

where, S_M, S_{Na}, S_K, S_{Ti}, S_{Si}, and S_O denote the Sanderson electronegativities of the exchanged metal ion, sodium, potassium, titanium, silicon, and oxygen, respectively.

Effects of Cation Electronegativity and Degree of Hydration on Chemical Shifts. Figure 4A shows that even in the fully hydrated state, the three chemical shifts $\delta(II_A)$, $\delta(II_B)$, and $\delta(III)$ experience gradual downfield shifts (to the left) with decreasing Sanderson electronegativity of the cation, in the order Sr^{2+}, Ba^{2+}, Na^+, $Na^+_{0.47} + K^+_{0.53}$, and K^+ (from bottom to top). Furthermore, in the case of Sr^{2+}-ETS-10, a new peak appears at around -99 ppm. We assign the peak as $\delta(II_B)$, which seems to be due to a very large upfield shift, as the results for the dry state make clear. Thus, in the dehydrated state, the gradual downfield shifts of the peaks with decreasing the Sanderson electronegativity of the cation become more straightforward (Figure 4B). In the dehydrated state, the very large upfield shift appears not only for Sr^{2+}-ETS-10 but also for Ba^{2+}-ETS-10. However, they merge into a pseudo-single peak in the hydrated state upon exchanging the Sr^{2+}, Ba^{2+}, $Na^+_{0.47} + K^+_{0.53}$, and K^+ ions with Na^+ (Figure 4C), indicating that the gradual shifts of $\delta(II_A)$, $\delta(II_B)$, and $\delta(III)$ do not arise from structural damage of ETS-10 that might have occurred during ion exchange. Thus, the above results clearly demonstrate that both the nature (elec-

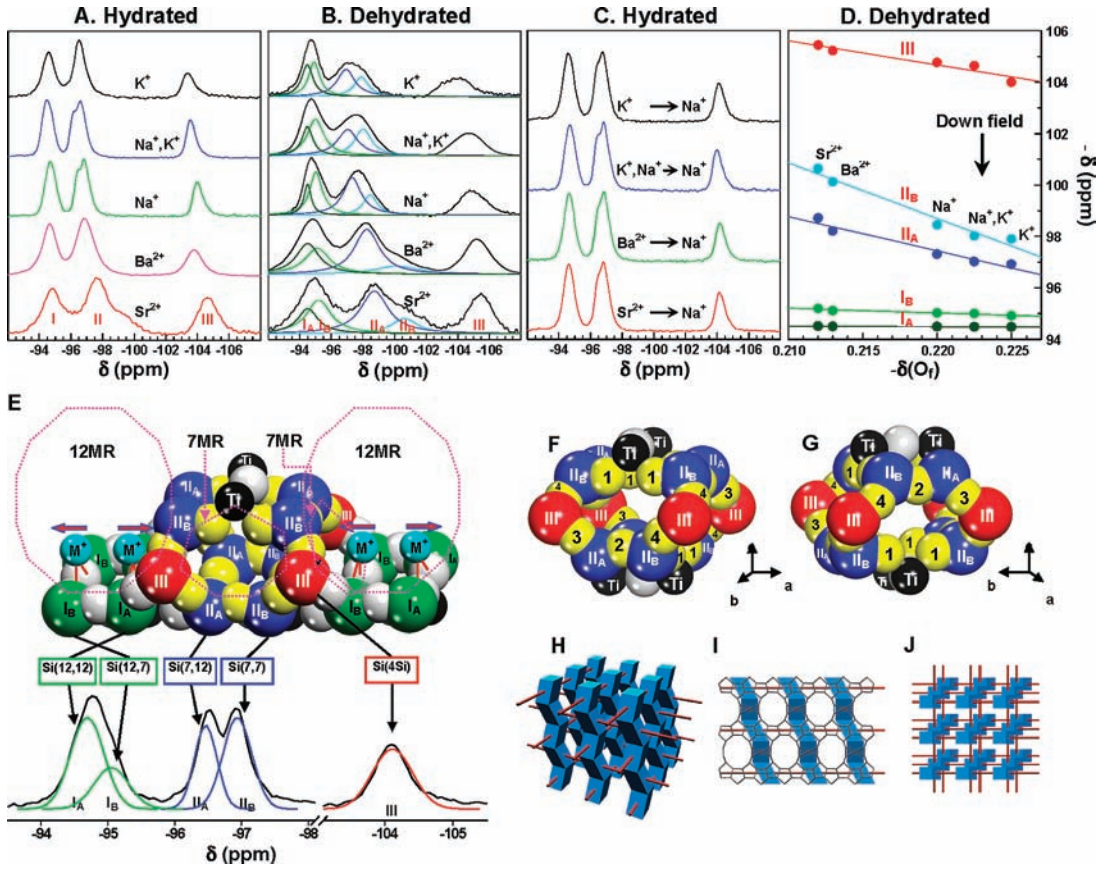

Figure 4. ^{29}Si solid-state MAS NMR spectra of M^{n+}-ETS-10 in the (A) hydrated and (B) dehydrated states and of (C) ($M^{n+}\rightarrow Na^+$)ETS-10 in the hydrated state. (D) Plot of the five chemical shifts described at the bottom of (B) vs $-\delta(O_f)$ for M^{n+} as indicated. (E) Illustration of the positions of the five different types of Si atoms near a $(7MR)_4$ cage in ETS-10 along a TiO_3^{2-} quantum wire and the correlation between the Si atoms and the NMR peaks (general description). (F, G) Illustrations of a $(7MR)_4$ cage in ETS-10 from two different perspectives, showing three different types of Si atoms and four different types of O atoms protruding into the interior of the cage. (H–J) Illustrations of cation-existing regions for the case of polymorph B as (H) a 3D perspective or as two-dimensional views along the (I) *a* or *b* or (J) *c* direction.

tronegativity) of the cation and the degree of hydration sensitively affect $\delta(II_A)$, $\delta(II_B)$, and $\delta(III)$.

Nonuniform Sensitivities of Chemical Shifts to Framework Oxide Charge Density. Figure 4D describes the following two very interesting phenomena. First, the chemical shifts of ^{29}Si shift downfield as $-\delta(O_f)$ increases. Second, the slopes in these linear relationships are not uniform: the absolute slope values {in ppm/[$-\delta(O_f)$]} are 2.5 for $\delta(I_A)$, 18.6 for $\delta(I_B)$, 133.5 for $\delta(II_A)$, 216.3 for $\delta(II_B)$, and 93.8 for $\delta(III)$, which increase in the order $\delta(I_A) \leq \delta(I_B) \ll \delta(III) < \delta(II_A) < \delta(II_B)$. Anderson and co-workers assigned $\delta(I_A)$, $\delta(I_B)$, $\delta(II_A)$, and $\delta(II_B)$ as the chemical shifts of four NMR-spectroscopically nonequivalent Si atoms connected to three Si atoms and one Ti atom [denoted as Si(3Si,1Ti)] and $\delta(III)$ as the chemical shift of the Si atom connected to four Si atoms [denoted as Si(4Si)].[1b,c] They also identified the four NMR-spectroscopically nonequivalent Si atoms in Si(3Si,1Ti) and named them as Si(12,12), Si(12,7), Si(7,12), and Si(7,7) on the basis of their connectivities to the adjacent 7MR and 12MR systems (Figure 4E). However, the one-to-one correlation between the four nonequivalent Si(3Si,1Ti) atoms [Si(12,12), Si(12,7), Si(7,12), and Si(7,7)] and the four chemical shifts [$\delta(I_A)$, $\delta(I_B)$, $\delta(II_A)$, and $\delta(II_B)$] has not been established to date. It will therefore further deepen our understanding of ETS-10 if there is a way to make a one-to-one correlation between the four chemical shifts and the four Si(3Si,1Ti) sites.

It should be recalled that the chemical shift of ^{29}Si shifts downfield as the charge density on the Si atom increases[25c,37] and that the negative charge density of the framework oxide increases with decreasing electronegativity of the charge-balancing cation for a given zeolite and with increasing degree of hydration of the zeolite (see above).[24–26] The latter result arises because increasing the degree of hydration leads to a decrease in the degree of direct LMCT interaction between the framework oxide and the cation (Scheme 1), which gives rise to a decrease in the degree of partial electron transfer from the framework oxide to the cation in the ground state.

Cation Locations: Uniform versus Nonuniform Cation Distributions. In ETS-10, there are V-shaped Si−O−Ti−O−Si units that repeat along the titanate quantum wires at the positions perpendicular to the quantum wire direction. The two Si atoms are equivalent, and they are positioned in four different environments depending on their connectivity to 7MRs and 12MRs (see above). Accordingly, there are four different types of Si−O−Ti−O−Si units, namely, Si(7,7)−O−Ti−O−Si(7,7), Si(7,12)−O−Ti−O−Si(7,12), Si(12,7)−O−Ti−O−Si(12,7), and Si(12,12)−O−Ti−O−Si(12,12). Among these, Si(7,7)−O−Ti−O−Si(7,7) and Si(7,12)−O−Ti−O−Si(7,12) units are located in a small cage produced by connecting two perpendicularly running adjacent titanate quantum wires through four Si(4Si) atoms (Figure 4E). Eventually, each cage becomes surrounded by two sets of confronting 7MR, windows and the confronting windows are mirror images of each other. We call this structure a $(7MR)_4$ cage on the basis of the fact that it is surrounded by four 7MRs. The other two units, Si(12,7)−O−Ti−O−Si(12,7) and Si(12,12)−O−Ti−O−Si(12,12), are located in 12MR channels (Figure 4E).

It has been proposed that in the case of monovalent cations, a cation exists in the vicinity of the two O atoms of a Si−O−Ti−O−Si unit, regardless of its type.[27] In fact, two Si−O−Ti−O−Si units share a Ti atom, forming the letter X [$(Si-O)_2-Ti-(O-Si)_2$]. As a result, two cations exist in the vicinity of each Ti center (in opposite positions) regardless of the type of Si−O−Ti−O−Si unit, giving rise to a uniform distribution of cations along the titanate wire. However, the "*uniform distribution model*" cannot account for the very large difference in the sensitivities of $\delta(I_A)$, $\delta(I_B)$, $\delta(II_A)$, $\delta(II_B)$, and $\delta(III)$ to the variation of $-\delta(O_f)$ (Figure 4D), particularly the fact that the sensitivities of $\delta(I_A)$ and $\delta(I_B)$ are negligible and very small, respectively. We attribute such a large difference in sensitivities to the *nonuniform distribution* of countercations along the titanate (TiO_3^{2-}) molecular wires in the dehydrated state.

Migration of Cations from 12MR Channels to $(7MR)_4$ Cages upon Dehydration. We now propose that the above cations that may exist near Si(12,7)−O−Ti−O−Si(12,7) and Si(12,12)−O−Ti−O−Si(12,12) in the 12MR in the hydrated state migrate into the neighboring $(7MR)_4$ cages through the 7MR windows (Figure 4E) upon dehydration.[38] Since the cations can have 3D coordination to the oxygen atoms (yellow) in a $(7MR)_4$ cage, we believe that the increase in coordination number is the driving force for the above phenomenon. As a result, upon dehydration, Si(12,12) (green, marked as I_A) and Si(12,7) (green, marked as I_B) atoms existing in 12MR channels should experience very low degrees of electron density depletion, since the cations do not coordinate to the O atoms adjacent to the Si(12,12) and Si(12,7) atoms. On the other hand, upon dehydration, all of the framework Si atoms that form a $(7MR)_4$ cage, namely, Si(7,12) (blue, marked as II_A), Si(7,7) (blue, marked as II_B), and even Si(4Si) (red, marked III), should experience much higher degrees of electron density removal because of the influx of additional cations into the $(7MR)_4$ cage, which should eventually deplete additional electron density from the three types of Si atoms through coordination to the oxygen atoms. Accordingly, Si(7,7), Si(7,12), and Si(4Si) atoms should be very sensitively affected by the type of countercation, while Si(12,12) and Si(12,7) atoms in the dehydrated state should not.

Assignment of Four ^{29}Si Chemical Shifts to Four Si(3Si,1Ti) Atoms. On the basis of the above "*nonuniform distribution model*", we conclude that $\delta(I_A)$, $\delta(I_B)$, $\delta(II_A)$, and $\delta(II_B)$ arise from Si(12,12), Si(12,7), Si(7,12), and Si(7,7), respectively, as illustrated in Figure 4E (also see Figure SI 3 in the Supporting Information). The following further supports the above conclusion. Among the Si(7,7) and Si(7,12) atoms, the latter are placed closer to the oxygen atoms connected to Si(12,7) atoms, to which the cations do not bind. Therefore, we assign $\delta(II_A)$ to Si(7,12) and the most sensitive shift, $\delta(II_B)$, to Si(7,7). Likewise, we assign the least sensitive shift, $\delta(I_A)$, to Si(12,12) and $\delta(I_B)$ to Si(12,7).

(37) (a) Melchior, M. T.; Vaughan, D. E. W.; Jarman, R. H.; Jacobson, A. J. *Nature* **1982**, *298*, 455–456. (b) Dyer, A. In *An Introduction to Zeolite Molecular Sieves*; John Wiley & Sons: New York, 1988; Chapter 4.

(38) We also obtained ^{29}Si MAS NMR spectra of M^{n+}-ETS-10 for $M^{n+} = Ca^{2+}$, Cd^{2+}, Pb^{2+}, and Zn^{2+}, cations that are more electronegative than those shown in Figure 4. In these samples, contrary to the results for K^+, Na^+, Ba^{2+}, and Sr^{2+}, the two peaks I and II merge into single peaks with centers appearing between −96 and −98 ppm; this is due to more pronounced shift upfield (to the right) for peak I than peak II. This phenomenon indicates that in the case of the more electronegative cations (Ca^{2+}, Cd^{2+}, Pb^{2+}, Zn^{2+}), the cations that already exist in the 12MR in the hydrated state tend to remain in the same ring even after dehydration. However, because of the difficulty in resolving the single peaks into four peaks (I_A, I_B, II_A, and II_B), we could not extract the details. Since this work already contains a large number of complicated results, we will study the effect of the more electronegative cations on the ^{29}Si chemical shifts more rigorously and report the results later elsewhere.

Clustering of Cations in $(7MR)_4$ Cages. A $(7MR)_4$ cage is composed of four Ti atoms (black), four Si(7,12) atoms (blue, II_A), four Si(7,7) atoms (blue, II_B), four Si(4Si) atoms (red), 20 O atoms (yellow) that can coordinate to the interior cations, and two axial O atoms that connect two Ti atoms (gray) (Figure 4F,G). Out of the 20 coordinating O atoms, eight equatorial O atoms (labeled 1) are equivalent, as are four O atoms that connect Si(7,12) and Si(7,7) atoms (labeled 2), four O atoms that connect Si(4Si) and Si(7,12) atoms (labeled 3), and four O atoms that connect Si(4Si) and Si(7,7) atoms (labeled 4). In the case of monovalent cations, the cation population in a $(7MR)_4$ cage is eight, indicating the possibility that the cations form ionic clusters within the cage as a result of the space limitation inside the cage. The formation of ionic clusters should be confirmed.

Periodic Localization of Cations at the Cross Sections of the Titanate Quantum Wires. On the basis of the above, for the case of polymorph B, a 3D representation of the regions in which the cations exist in the dehydrated state is shown in Figure 4H; a 2D representation of these regions along the *a* or *b* axis is given in Figure 4I and one along the *c* axis in Figure 4J. These illustrations show that the cations exist only in the regions where two perpendicular titanate quantum wires cross in the dehydrated state, or at the cross sections of the titanate quantum wires. The corresponding illustrations for polymorph A are shown in Figure SI 4 in the Supporting Information. Thus, the above results reveal that along the titanate quantum wire, there are cation-coordinated and cation-absent regions in the dehydrated ETS-10. We believe that this finding will help elucidate more interesting features of ETS-10 in the future.

Usefulness of Surface Coating of Dry ETS-10 with Octadecyltrichlorosilane. The groups of Schmidt[30] and others[1b,c,28,31b,32,34,35] have also reported ^{29}Si NMR spectra of M^{n+}-ETS-10 with $M^{n+} = Na^+$, $Na^+_{0.47} + K^+_{0.53}$, K^+, and Cs^+. However, these groups were not able to elucidate the effects of the cation and degree of hydration on the shift in the chemical shift because of experimental difficulties in obtaining solid-state ^{29}Si NMR spectra of dehydrated samples. We attribute our successful elucidation of the above phenomena in the dehydrated state to the ability to preserve the fully dehydrated ETS-10 samples as such even in the ambient environments by coating the surfaces of the dehydrated samples with octadecyltrichlorosilane.[33] This method has also proved to be useful for obtaining powder XRD patterns of dehydrated zeolites.[33]

XPS Studies of M^{n+}-ETS-10. XPS spectra of Ti(2p) and O(1s) were obtained from M^{n+}-ETS-10 with $M^{n+} = K^+$, Na^+, Ba^{2+}, Sr^{2+}, and Ca^{2+}. The XPS spectrum of Ti(2p) is supposed to give two peaks due to the two spin−orbit-coupled energy states, $J = {}^3/_2$ and ${}^1/_2$, with the former appearing in the lower-energy region and the latter in the higher-energy region. The XPS spectra for Ti(2p) in M^{n+}-ETS-10 (Figure 5A) clearly indicate that there are two peaks in each of these energy regions, indicating that there are two Ti species, I and II. The binding energies for each species are listed in Table SI 6 in the Supporting Information. The higher-energy peak for the ${}^3/_2$ state appears at 458.1−458.9 eV, a typical region for Ti^{4+}, while the lower-energy peak appears at 456.5−457.6 eV, a typical region for Ti^{3+}. We therefore assign the XPS peaks as $Ti^{3+}({}^3/_2)$, $Ti^{4+}({}^3/_2)$, $Ti^{3+}({}^1/_2)$, and $Ti^{4+}({}^1/_2)$, respectively. The $Ti^{3+}({}^3/_2)$/$Ti^{4+}({}^3/_2)$ intensity ratios were between 1.0:1.5 and 1.0:2.7, and the $Ti^{3+}({}^1/_2)$/$Ti^{4+}({}^1/_2)$ intensity ratios were between 1.0:0.6 and 1.0:1.9.

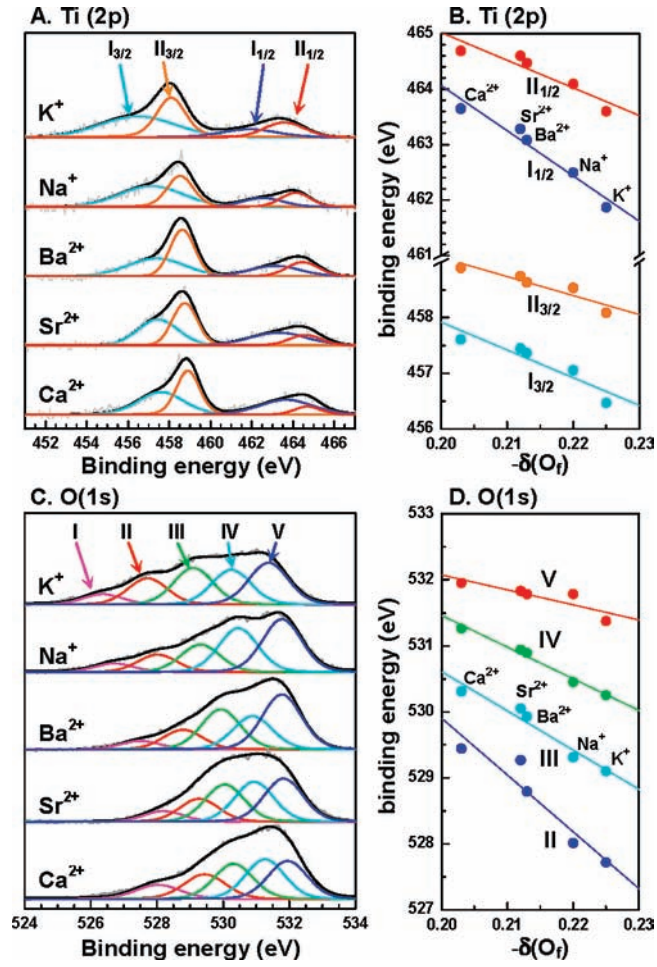

Figure 5. (A) XPS spectra of M^{n+}-ETS-10 (with M^{n+} as indicated) in the Ti(2p) region, showing two different types of Ti. (B) Plot of the Ti(2p) binding energies vs $-\delta(O_f)$ for various M^{n+}. (C) XPS spectra of M^{n+}-ETS-10 in the O(1s) region, showing five different types of O. (D) Plot of the O(1s) binding energies vs $-\delta(O_f)$ for various M^{n+}.

Scheme 2

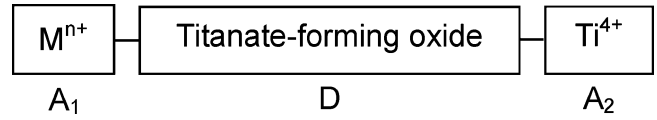

Triad Interaction between the Cation, Oxide, and Ti(IV). The peaks gradually shifted to the higher-energy region with increasing electronegativity of the countercation, indicating that cations are removing electron density from the Ti species. The plot of the binding energies of the two Ti species versus $-\delta(O_f)$ (Figure 5B) reveals that the Ti(2p) binding energies decrease linearly as $-\delta(O_f)$ increases, indicating that the electron density on Ti increases as the (average) negative charge density of the framework oxygen increases. This phenomenon also shows that oxide-to-titanium(IV) LMCT occurs from the oxide ions to the titanium(IV) ions in the titanate quantum wire, even in the ground state. Overall, the above results show that M^{n+}, titanate-forming oxide, and Ti^{4+} form an acceptor 1−donor−acceptor 2 (A_1−D−A_2) triad system, as shown in Scheme 2.

Interestingly, the sensitivity of Ti^{3+} to the electronegativity of the cation was higher than that of Ti^{4+}. We believe this happens because the Ti^{3+} species are richer in electron density than Ti^{4+}. It may also occur because of the presence of the Ti^{3+} centers in the $(7MR)_4$ cage region, where the cation population

is high. We believe that the latter explanation is more compelling, since the Ti^{3+} centers can be stabilized more as a result of their location in the $(7MR)_4$ cage.

Highly Basic Framework Oxide. The appearance of significant amounts of Ti^{3+} from M^{n+}-ETS-10 is quite interesting since the related bulk titanate materials (Na_2TiO_3, $CaTiO_3$, and $BaTiO_3$) do not show the Ti^{3+} peak in the XPS spectra.[39−41] We believe that the Ti^{3+} species are produced during XPS measurements in the vacuum chamber by X-ray-(photo)induced O-to-Ti charge transfer, since we did not detect the ESR signal of Ti^{3+} from the dehydrated ETS-10 under vacuum. Therefore, the different behaviors of ETS-10 and bulk titanates indicate that the oxide species in titanate quantum wires are much more basic than those of bulk 3D titanates, as will be discussed in more detail later in this work. The formation of significant amounts of Ti^{3+} species may also be possible as a result of the likely stabilization of the extra electron on Ti with charge-balancing cations clustered within the $(7MR)_4$ cages. This interpretation is consistent with the fact that the sensitivity of Ti^{3+} to the electronegativity of the cation is higher than that of Ti^{4+} (see above).

Spin−Orbit Splitting of Ti. The measured spin−orbit splitting $[\Delta(2p_{3/2} - 2p_{1/2})]$ values for Ti^{4+} ions were 5.51, 5.55, 5.83, 5.85, and 5.79 eV for $M^{n+} = K^+$, Na^+, Ba^{2+}, Sr^{2+}, and Ca^{2+}, respectively, and those for Ti^{3+} ions were 5.40, 5.43, 5.71, 5.83, and 6.04 eV for $M^{n+} = K^+$, Na^+, Ba^{2+}, Sr^{2+}, and Ca^{2+}, respectively. Thus, the degree of spin−orbit splitting increases as the electronegativity of the cation increases and hence as the charge densities of O and Ti atoms decrease. This result indicates that the effective nuclear charge of the Ti atom increases as the electronegativity of the charge-balancing cation increases because the degree of spin−orbit splitting of an atom increases as the effective nuclear charge of the atom increases.[42] The above result further indicates that the depletion of electron density from the oxide by the charge-balancing cation sequentially leads to the depletion of electron density from the Ti atom, giving rise to the increase in the effective nuclear charge of the Ti atom, and that the degree of electron density depletion from the Ti atom increases as the electronegativity of the charge balancing cation increases. This phenomenon also serves as direct evidence that M^{n+}, titanate-forming oxide, and Ti^{4+} form a triad complex as shown in Scheme 2.

The available literature values for the spin−orbit splitting of bulk 3D titanates are 5.8,[39] 5.6,[41] 6.0,[40] and 5.6[43] eV for Na_2TiO_3, $BaTiO_3$, $CaTiO_3$, and $PbTiO_3$, respectively. As noted, the degree of spin−orbit splitting does not increase with increasing electronegativity of the cation, unlike the case of the titanate quantum wire in ETS-10. We suspected that the absence of a trend for the bulk 3D titanates could arise from the fact that the values were obtained from different laboratories, so we measured XPS spectra of the bulk 3D titanates Li_2TiO_3, $BaTiO_3$, $SrTiO_3$, $CaTiO_3$, and $PbTiO_3$ and obtained the corresponding spin−orbit splitting values, which are 5.74, 5.78, 5.81, 5.74, 5.76 eV (see Table SI 7 in the Supporting Information for more details). Again, we could not find any trend for the bulk 3D titanates. Such an absence of the trend for the bulk 3D titanates may arise from the different M−O (where M is the counter-cation) and O−Ti bond lengths, since the degree of charge transfer is sensitively affected by the distance between the donor and acceptor. In any case, it is clear that the titanate quantum wire in ETS-10 is unique in the sense that it shows a systematic change of the degree of spin−orbit splitting as the electronegativity of the charge-balancing cation changes.

It is noteworthy that the spin−orbit splitting values (in eV) of the 3D titanate and 1D ETS-10 titanate quantum wire for Ti^{4+} are similar for a given cation: 5.83 and 5.78 for Ba^{2+}, 5.85 and 5.81 for Sr^{2+}, and 5.79 and 5.74 for Ca^{2+}. Thus, the spin−orbit splitting does not change upon reduction of the dimensionality from 3D in the bulk to 1D in the titanate quantum wire in ETS-10. This result contrasts with the case of $PbTiO_3$, whose spin−orbit splitting value increases markedly (by 0.9 eV) in going from the 3D bulk (5.6 eV)[41] to the 1D nanowire (6.5 eV),[44] indicating that the degree of electron depletion from Ti by Pb^{2+} increases markedly as the dimensionality decreases. The lack of such a marked increase in spin−orbit splitting in going from the 3D bulk titanate to the 1D titanate quantum wire in ETS-10 may arise from the open nature of the ETS-10 structure, in which the cations next to the titanate quantum wires do not bind to the oxide ions as tightly as in the case of the 1D nanowire.

XPS spectra of O(1s). The XPS spectra for O(1s) in M^{n+}-ETS-10 (Figure 5C) reveal that there are at least five different types of O species in terms of binding energy. The binding energies for each of these species ranged from 526.1 to 531.9 eV, and the values are listed in Table SI 6 in the Supporting Information. We believe the lower-binding-energy species are the oxide species that form titanate quantum wires. Interestingly, the binding energies of O(1s) of the oxygen atoms in the titanate quantum wires are significantly lower than those of O(1s) of various metal-ion-exchanged zeolites (530.2−533.3 eV),[24] indicating that the oxide ions in the quantum wires are much more basic than the zeolite framework oxides. The values are also significantly lower than those of bulk titanates, which range between 529 and 531 eV.[39,41,44,45] This explains why titanate quantum wires are so much vulnerable to acid,[31] even to NH_4^+ ion,[28,30] which can easily generate H^+ after liberation of NH_3 even under mild conditions, and also to H_2O_2, which is a typical oxidant.[13b,35] The plot of the O(1s) binding energies versus $-\delta(O_f)$ (Figure 5D) shows that the binding energies of O(1s) decrease linearly as $-\delta(O_f)$ increases, despite the fact that O(1s) is a core-level electron.

Effects of Cation and Degree of Hydration on the Raman Spectra of Titanate Quantum Wires. Background. As described earlier (see above), it is of interest to study the effect of various cations other than H^+ and NH_4^+ on the longitudinal stretching vibration of the titanate quantum wire. The aforementioned fact that the electronegativity of the charge-balancing cation and the degree of hydration sensitively affect the negative charge density of the titanate quantum wire further provides us a good opportunity to elucidate the effect of the cation and the degree of hydration on the frequency and bandwidth of the longitudinal stretching vibration of the titanate quantum wire and to analyze

(39) Chu, C. L.; Chung, C. Y.; Zhou, J.; Pu, Y. P.; Lin, P. H. *J. Biomed. Mater. Res.* **2005**, *75A*, 595–602.
(40) Wiff, J. P.; Fuenzalida, V. M.; Zárate, R. A.; Arias, J. L.; Fernández, M. S. *J. Phys.: Condens. Matter* **2004**, *16*, S1345–S1350.
(41) (a) Jin, Y.; Zhu, Y.; Yang, X.; Li, C.; Zhou, J. *J. Solid State Chem.* **2007**, *180*, 301–306. (b) López, M. D. C. B.; Fourlaris, G.; Rand, B.; Riley, F. L. *J. Am. Ceram. Soc.* **1999**, *82*, 1777–1786.
(42) Atkins, P. W. In *Physical Chemistry*, 6th ed.; Oxford University Press: Oxford, U.K., 1998; p. 374.
(43) Kim, J.-N.; Shin, K.-S.; Park, B.-O.; Lee, J.-H.; Kim, N.-K.; Cho, S.-H. *Smart Mater. Struct.* **2003**, *12*, 565–570.
(44) Gu, H.; Hu, Y.; You, J.; Hu, Z.; Yuan, Y.; Zhang, T. *J. Appl. Phys.* **2007**, *101*, 024319.
(45) Meng, X.-D.; Wang, D.-Z.; Liu, J.-H.; Zhang, S.-Y. *Mater. Res. Bull.* **2004**, *39*, 2163–2170.

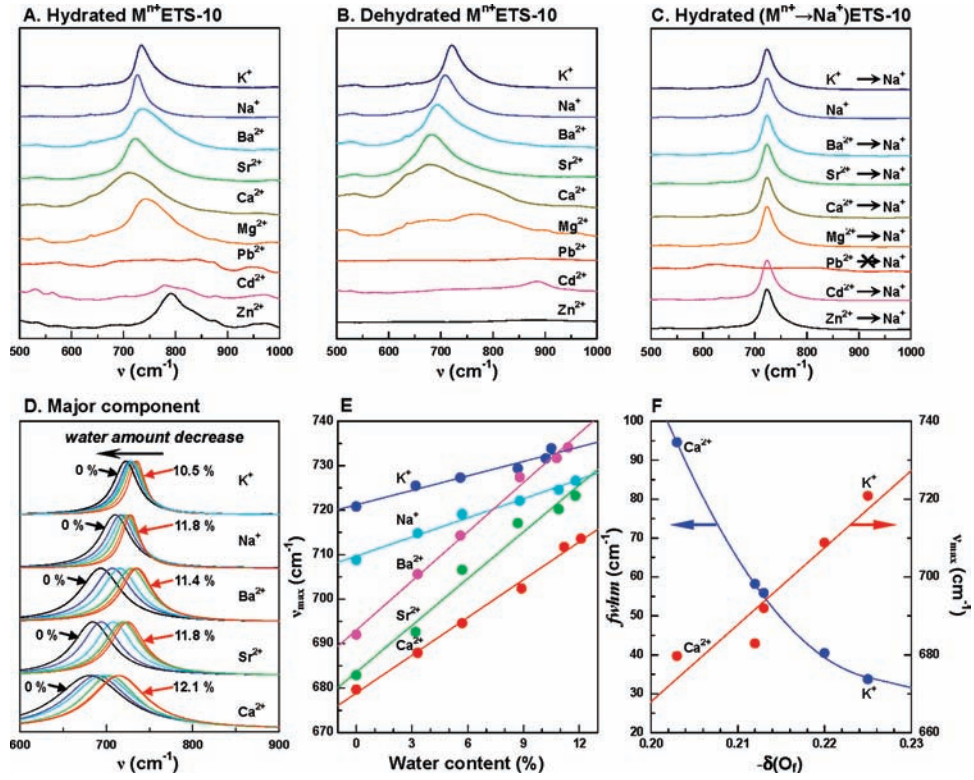

Figure 6. Raman spectra of M^{n+}-ETS-10 (M^{n+} as indicated) in the (A) hydrated and (B) dehydrated states and of (C) (M^{n+}→Na^+)ETS-10 in the 500−1000 cm^{-1} region. (D) Major components of the along-the-wire vibrational bands of M^{n+}-ETS-10 (for five M^{n+}, as indicated) with varying water content (from the fully hydrated states to the fully dehydrated states). (E) Plots of the frequencies of along-the-wire vibrational bands with respect to water content for various M^{n+}. (F) Plots of the frequencies and bandwidths of the along-the-wire vibrational bands of fully dehydrated M^{n+}-ETS-10 with respect to $-\delta(O_f)$.

the results in the context of the effect of the charge density of the quantum wire on its vibrational frequency and bandwidth.

One of the ultimate aims of current nanotechnology is to utilize metallic and semiconducting quantum wires as building blocks for nanoscale electronic devices and other novel applications.[18,19,46,47] However, because of their extremely small thicknesses (on the order of molecular dimensions), the charge-transfer (CT) interaction between the environment and the quantum wire significantly affects the physical properties of the molecular wire through charge injection from the environment into the quantum wire.[47] One of the important effects is the change in vibrational frequency of the quantum wire in response to charge injection from the environment. Thus, in the cases of SW-CNTs, it has been shown that electron injection into the nanotubes significantly affects their vibrational frequencies and bandwidths.[47] As the vibrational frequency significantly affects their performance during applications, the elucidation of the effects of various environments on the vibrational frequency and bandwidth is of great importance. However, studies of such effects have been limited to SW-CNTs.[47a] Therefore, their elucidation in the case of titanate quantum wires will help us deepen our understanding of the fundamental properties of quantum wires, which is essential for the novel application of the these wires in future nanodevices. In this regard, we also studied the effect of the environment (the nature of cation and the degree of hydration) on the vibrational frequency and bandwidth of the titanate quantum wires.

Effects of Cation and Degree of Hydration on the Stretching Vibrations of Titanate Quantum Wires. The Raman spectrum of hydrated M^{n+}-ETS-10 changes markedly as M^{n+} is changed (Figure 6A). Most notably, the longitudinal vibrational peak of the titanate quantum wire shifts irregularly to either the lower- or higher-frequency region (for $M^{n+} = K^+$, Na^+, Ba^{2+}, Sr^{2+}, Ca^{2+}, Mg^{2+}, Zn^{2+}) or even disappears (for $M^{n+} = Pb^{2+}$, Cd^{2+}). Upon dehydration, the vibrational band gradually shifts to the lower-energy region, and its bandwidth (fwhm) progressively increases with increasing Sanderson electronegativity for $M^{n+} = K^+$, Na^+, Ba^{2+}, Sr^{2+}, and Ca^{2+} (Figure 6B). When $M^{n+} = Mg^{2+}$, the vibrational band intensity decreases significantly, and when $M^{n+} = Pb^{2+}$, Cd^{2+}, or Zn^{2+}, the vibrational band nearly or completely disappears. However, upon reverse-exchange of M^{n+} with Na^+, the Raman spectra become identical with that of Na^+-ETS-10, except when $M^{n+} = Pb^{2+}$ (Figure 6C), indicating that the titanate quantum wires were not damaged during or after ion exchange or after dehydration. The nonreappearance of the Raman band of the titanate quantum wire in the case of $M^{n+} = Pb^{2+}$ arises from the difficulty of reverse-exchanging Pb^{2+} with Na^+.

The longitudinal stretching vibration frequency of the titanate quantum wire gradually shifts to the lower-frequency region and the bandwidth gradually increases as the water content decreases from ~12 to 0% for $M^{n+} = K^+$, Na^+, Ba^{2+}, Sr^{2+}, and Ca^{2+} (Figure SI 5 and Table SI 8 in the Supporting

(46) (a) Kan, S.; Mokari, T.; Rothenberg, E.; Banin, U. *Nat. Mater.* **2003**, *2*, 155–158. (b) Ahrenkiel, S. P.; Miedaner, O. I.; Curtis, C. J.; Nedeljković, J. M.; Nozic, A. J. *Nano Lett.* **2003**, *3*, 833–837. (c) Ouyang, M.; Huang, J.-L.; Lieber, C. M. *Acc. Chem. Res.* **2002**, *35*, 1018–1025.

(47) (a) Tsang, J. C.; Freitag, M.; Perebeinos, V.; Liu, J.; Avouris, P. H. *Nat. Nanotechnol.* **2007**, *2*, 725–730. (b) Shim, M.; Ozel, T.; Gaur, A.; Wang, C. *J. Am. Chem. Soc.* **2006**, *128*, 7522–7530. (c) Rao, A. M.; Eklund, P. C.; Bandow, S.; Thess, A.; Smalley, R. E. *Nature* **1997**, *388*, 257–259.

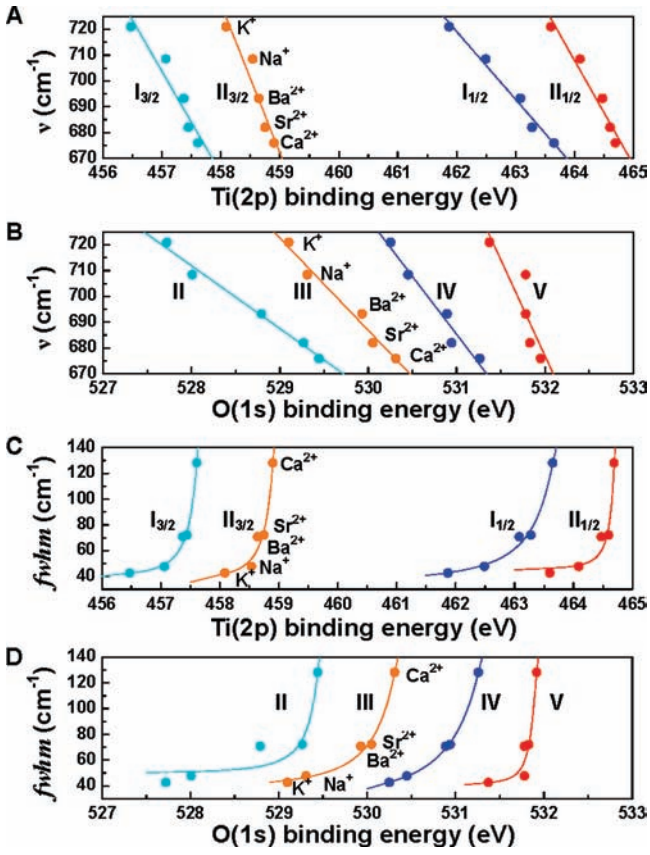

Figure 7. Plots of the along-the-wire vibrational frequencies of M^{n+}-ETS-10 (for five M^{n+}, as indicated) versus the binding energies of (A) Ti(2p) and (B) O(1s), and plots of the along-the-wire vibrational bandwidths of M^{n+}-ETS-10 (for five M^{n+}, as indicated) with respect to the binding energies of (C) Ti(2p) and (D) O(1s). The slopes in (A) are −39.7, −57.7, −26.3, and −40.5 cm^{-1}/eV from left to right, and those in (B) are −24.4, −35.8, −45.1, and −74.6 cm^{-1}/eV from left to right.

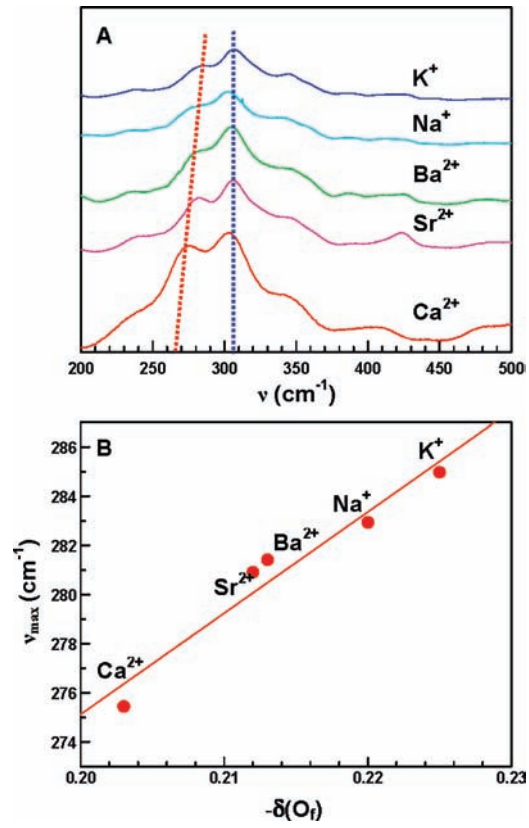

Figure 8. (A) Raman spectra of fully dehydrated M^{n+}-ETS-10 (M^{n+} as indicated) in the 200−500 cm^{-1} region and (B) the linear relationship between $-\delta(O_f)$ and the frequency of the band at 274−280 cm^{-1}.

Information). Since each vibrational spectrum has at least two components and there are other additional small peaks that overlap the main component of the vibrational band in the case of Ca^{2+}-ETS-10, we extracted the main component from each spectrum by deconvolution and compared only the extracted main components for a given water content in Figure 6D. This panel clearly shows that the frequency is progressively red-shifted and the bandwidth progressively increases as the water content decreases. In the fully dehydrated states, the vibrational frequencies are 720.8, 708.8, 692.0, 682.9, and 679.7 cm^{-1} and the bandwidths (fwhm) are 33.7, 40.4, 55.9, 58.2, 94.6 cm^{-1} for K^+, Na^+, Ba^{2+}, Sr^{2+}, and Ca^{2+}, respectively.

Linear Relationship between the Stretching Vibrational Frequency and Water Content and the Metallic Nature of the Titanate Quantum Wires. Interestingly, for each M^{n+}, the longitudinal stretching vibration frequency and the water content show a linear relationship, as shown in Figure 6E. It also shows that the sensitivity of the peak shift with respect to the water content increases in the order $K^+ \leq Na^+ \ll Ca^{2+} < Sr^{2+} \leq Ba^{2+}$. Thus, the sensitivity is higher for divalent cations than monovalent ones, despite the fact that the number of divalent cations is half that of the monovalent ones, and the sensitivity increases with increasing size of the divalent cation. This also makes clear that the degree of direct binding of the metal cation to the oxide framework increases in the same order as the water content decreases. Plots of the longitudinal vibrational frequency and the bandwidth versus $-\delta(O_f)$ for the fully dehydrated states are shown in Figure 6F, which reveals a very interesting linear relationship between the longitudinal vibrational frequency of the titanate quantum and $-\delta(O_f)$ and the fact that the bandwidth decreases nonlinearly as $-\delta(O_f)$ increases. This behavior of the titanate quantum wire is similar to that of metallic SW-CNTs in the sense that the vibrational frequency increases and the bandwidth decreases with increasing electron density.[47] Although the amounts of charge injection into the titanate quantum wire and SW-CNT cannot be directly compared, the sizes of the frequency increase (45 cm^{-1}) and bandwidth decrease (54 cm^{-1}) observed for the titanate quantum wire are much larger than those observed for metallic SW-CNTs (∼10 cm^{-1} and ∼20 cm^{-1}, respectively).[47]

The partial negative charge of the framework oxide, $-\delta(O_f)$, has successfully represented the negative charge density, electron donor strength, and basicity of the framework oxide. In many cases, the $-\delta(O_f)$ values have greatly helped explain the observed physical and chemical properties of zeolites, which are related to differences in the framework charge density, electron donor strength, and basicity. Nevertheless, $-\delta(O_f)$ is still a theoretical value. Therefore, wherever possible, attempts to correlate the observed physical and chemical properties with actual experimental values that can represent the charge density, electron donor strength, and basicity of the framework elements have to be made. In this work, the Ti(2p) and O(1s) binding energies are such values. We found that the longitudinal stretching frequency linearly increases as the binding energies of $Ti^{3+}(^3/_2)$, $Ti^{4+}(^3/_2)$, $Ti^{3+}(^1/_2)$, and $Ti^{4+}(^1/_2)$ decrease (Figure 7A) and as those of $O_{II}(1s)$, $O_{III}(1s)$, $O_{IV}(1s)$, and $O_V(1s)$ decrease (Figure 7B). The bandwidth decreases nonlinearly as the binding energies of $Ti^{3+}(^3/_2)$, $Ti^{4+}(^3/_2)$, $Ti^{3+}(^1/_2)$, and $Ti^{4+}(^1/_2)$ decrease

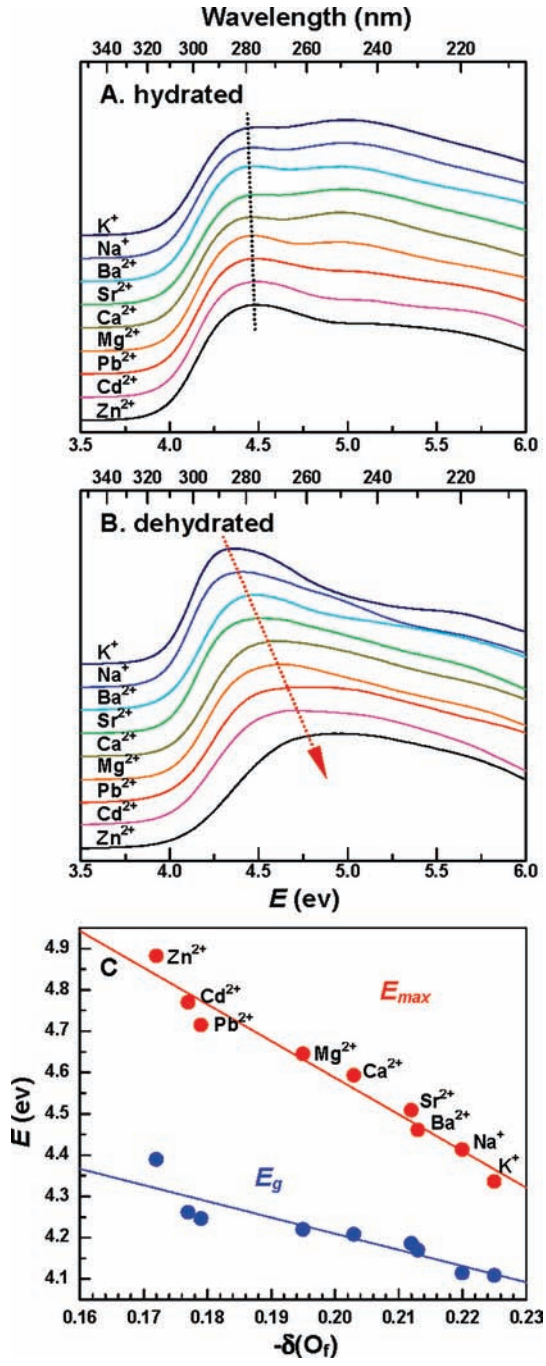

Figure 9. Diffuse reflectance spectra of M^{n+}-ETS-10 (M^{n+} as indicated) in the (A) hydrated and (B) dehydrated states, and (C) plots of the lowest-energy absorption maxima and the band-gap energies vs $-\delta(O_f)$ for the dehydrated states. The slopes in (C) are (top) −8.88 and (bottom) −3.92 eV/[$-\delta(O_f)$].

(Figure 7C) and as those of O_{II}(1s), O_{III}(1s), O_{IV}(1s), and O_V(1s) decrease (Figure 7D).

The fact that the vibrational frequency of the titanate quantum wire sensitively varies with changes in the water content further explains the observed discrepancies among the values for the Raman band of pristine ETS-10 samples in the literature,[13b,c,28,30–32,34,35] since the amount of adsorbed water varies from one laboratory to another depending on the relative humidity and the season. The fact that the stretching vibration frequencies of the titanate quantum wires of M^{n+}-ETS-10 change even in the fully hydrated states indicates that the cations, particularly large cations, cannot be fully hydrated by water molecules even in the fully hydrated state, presumably because of spatial restrictions.[25]

Thus, we have demonstrated for the first time that the charge density of the TiO_3^{2-} molecular wire in ETS-10 can be varied by varying the charge-balancing cation and the degree of hydration and that the longitudinal stretching vibration frequency of the titanate quantum wire increases linearly while the bandwidth of the vibrational band decreases nonlinearly as $-\delta(O_f)$ increases.

New Vibrational Mode of the Titanate Quantum Wire. In addition to the longitudinal stretching vibration band of the titanate quantum wire that appears between 600 and 800 cm^{-1}, we also paid attention to the three weaker, lower-energy Raman bands that appear in the 250−400 cm^{-1} region (Figure 8A). These bands have been proposed to arise from Ti−O−Ti bending vibrations.[48] If they indeed arise from the Ti−O−Ti bending vibrations, then they should also experience shifts to higher-energy regions with increasing negative charge density of the titanate quantum wire, as was the case for the longitudinal stretching vibration, since they also originate from the vibration of the titanate quantum wire. However, while the bands at 305 and 345 cm^{-1} remain almost unaltered, the band at 274−280 cm^{-1} progressively shifts to higher energy as the cation is changed from Ca^{2+} to K^+ (bottom to top in Figure 8A). The plot of the frequency with respect to $-\delta(O_f)$ shows a linear relationship (Figure 8B). This trend exactly matches that of the longitudinal stretching vibration of the titanate quantum wire. Accordingly, we propose that out of the three bands in the 250−400 cm^{-1} region, only the band at 274−280 cm^{-1} is another vibrational normal mode of the titanate quantum wire. We propose that this band arises from bending of the quantum wire, since it is significantly lower in energy than the longitudinal stretching vibration of the quantum wire.

Effect of Cation and Degree of Hydration on the UV−Vis Spectra of the Titanate Quantum Wire. The band-gap energy of the titanate quantum wire, E_g, has been known to decrease as the length increases.[12] Now it has become clear that for a given length, we can change the charge density and the stretching and bending vibration frequencies of the titanate quantum wire by changing the electronegativity of the cation and the degree of hydration. In fact, the longitudinal stretching and bending vibrations of the titanate quantum wire can be regarded as its longitudinal and transverse optical phonons, since titanate quantum wires are a part of a crystalline solid. In view of the fact that E_g is affected by phonons and the notion that an increase in charge density in a semiconductor material will affect the energy levels of its electronic bands, it is of great interest to investigate the relationship between the charge density of the titanate quantum wire and the electronic (UV−vis) spectra of M^{n+}-ETS-10 for various M^{n+} in both the hydrated and dehydrated states.

In the hydrated states, the spectra remain almost the same, except for a slight shift of the lowest-energy absorption maximum to higher energy as the cation is changed according to the order shown in Figure 9A. As a result, E_g also remains the same at 4.03 eV.[49] This again confirms that hydration of the cations prevents the direct LMCT from the framework to the cation. Lamberti[15] has also reported that the UV−vis

(48) Hong, S. B.; Kim, S. J.; Uh, Y. S. *Korean J. Chem. Eng* **1996**, *13*, 419–421.

(49) The E_g values were determined from the inflection points of the UV−vis spectra of the M^{n+}-ETS-10 samples (Figure 9B).

spectrum of ETS-10 remains the same regardless of the cation (among K^+, Li^+, Ca^{2+}, and Ba^{2+}), indicating that the investigated ETS-10 samples were fully hydrated.

Negative Linear Relationship between E_g and Partial Negative Charge of the Framework Oxide. The UV−vis spectrum of ETS-10 is blue-shifted as dehydration proceeds, as shown in Figure SI 6 in the Supporting Information. In the fully dehydrated states, the lowest-energy absorption maximum becomes distinct and progressively shifts to higher energies [from 4.34 eV (286 nm) to 4.88 eV (254 nm)] as M^{n+} is changed from K^+ to Zn^{2+}, i.e., the Sanderson electronegativity of the cation increases (Figure 9B). Accordingly, E_g also progressively shifts from 4.11 to 4.39 eV. The plots of E_g and the energy of the lowest-energy absorption maximum, E_{max}, versus $-\delta(O_f)$ give negative linear relationships with slopes of −8.9 and −3.9 eV/[$-\delta(O_f)$], respectively (Figure 9C).

The fact that E_g and E_{max} decrease as $-\delta(O_f)$ increases indicates that the valence band has strong oxide character and the conduction band strong Ti(IV) character and that the lowest-energy absorption arises from oxide-to-Ti^{4+} LMCT, consistent with the proposals of Zecchina and co-workers.[13a,14,17] However, in the case of the latter, it is still not clear whether the LMCT arises from the equatorial or axial oxide ions to Ti(IV) ions. In any case, the above results clearly show that E_g and the lowest-energy absorption sensitively change with changes in the electronegativity of the cation and the degree of hydration. This work thus reveals that not only the length of the quantum wire[12] but also $-\delta(O_f)$ sensitively affect its E_g and lowest-energy absorption. Since $-\delta(O_f)$ is sensitively governed by the nature of the cation, this result further confirms the A_1-D-A_2 triad interaction between the charge-balancing cation, the titanate-forming oxide, and the titanium ion in the dry state (Scheme 2).

Summary

Overall, this work reports that in ETS-10, the charge-balancing cation, the titanate-forming oxide, and the titanium ion interact via acceptor 1−donor−acceptor 2 triad interaction (Scheme 2). Accordingly, the negative charge density of the titanate quantum wire can be finely tuned by varying the electronegativity and degree of hydration of the charge-balancing cation. For instance, the negative charge density of the titanate quantum wire can be decreased by increasing the electronegativity of the cation and/or decreasing the degree of hydration of the cation. The XPS data for Ti(2p) and O(1s) confirm the above behavior and also reveal that the oxide ions of the titanate quantum wires are much more basic than those of zeolites and the 3D titanates. The longitudinal stretching vibration frequency of the titanate quantum wire increases linearly while the Raman bandwidth decreases nonlinearly as the negative charge density of the titanate quantum wire increases, indicating that the titanate quantum wire is similar to a metallic SW-CNT. We also found another normal vibrational mode of the titanate quantum wire with a vibrational frequency of 274−280 cm^{-1}, which we have assigned as the bending vibration of the quantum wire. In the dehydrated state, E_g and the first absorption maximum shift to lower energy as the negative charge density of the oxide increases, indicating the oxide-to-titanium(IV) charge-transfer nature of the transitions. We have also shown that the cations existing in the 12MR channels migrate to the $(7MR)_4$ cages upon dehydration of ETS-10. On the basis of this phenomenon, we have assigned $\delta(I_A)$, $\delta(I_B)$, $\delta(II_A)$, and $\delta(II_B)$ as the chemical shifts arising from the Si(12,12), Si(12,7), Si(7,12), and Si(7,7) atoms, respectively.

Acknowledgment. We thank the Ministry of Education, Science, and Technology (MEST) of the Korean Government and Sogang University for supporting this work through the Acceleration Research and Internal University Research Programs. J.-H.P. and C.-H.S also thank the Carbon Dioxide Reduction & Sequestration Research Center, a 21st Century Frontier Program supported by MEST. H.C. and H.L. also thank the Quantum Photonic Science Research Center supported by MEST.

Supporting Information Available: Various tables, thermal stability of the titanate quantum wire, Ar adsorption isotherms, 2D illustration (along the *a* axis) of the positions of the five different types of Si atoms and the correlation between the Si atoms and the NMR peaks, illustrations of cation-existing regions in polymorph A, Raman spectra of M^{n+}-ETS-10 with varying degrees of hydration (raw data), and diffuse reflectance spectra of M^{n+}-ETS-10 with varying degrees of hydration. This material is available free of charge via the Internet at http://pubs.acs.org.

JA903638V